

One-dimensional Rashba states with unconventional spin texture in Bi chains

P. M. Sheverdyaeva¹, D. Pacilè^{2*}, D. Topwal^{3,4}, U. Manju⁵, M. Papagno², V. Feyrer⁶, M. Jugovac^{1,6†}, G. Zamborlini⁶, I. Cojocariu⁶, C. Tusche^{6,7}, X. L. Tan⁶, K. Hagiwara⁶, Y. J. Chen^{6,7}, J. Fujii⁸, P. Moras¹, L. Ferrari¹, E. Vescovo⁹, G. Bihlmayer¹⁰, and C. Carbone¹

¹ *Istituto di Struttura della Materia-CNR (ISM-CNR), SS 14, Km 163,5, I-34149, Trieste, Italy*

² *Dipartimento di Fisica, Università della Calabria, 87036 Arcavacata di Rende (CS), Italy*

³ *Homi Bhabha National Institute, Training School Complex, Anushakti Nagar, Mumbai 400094, India*

⁴ *Institute of Physics, Sachivalaya Marg, Bhubaneswar 751005, India*

⁵ *CSIR - Institute of Minerals and Materials Technology, Bhubaneswar 751013, India*

⁶ *Peter Grünberg Institut PGI, Forschungszentrum Jülich, 52425 Jülich, Germany*

⁷ *Fakultät für Physik, Universität Duisburg-Essen, Duisburg 47057, Germany*

⁸ *Istituto Officina dei Materiali (IOM)-CNR, Laboratorio TASC, Area Science Park, S.S.14, Km 163.5, 34149 Trieste, Italy*

⁹ *National Synchrotron Light Source, Brookhaven National Laboratory, Upton, New York 11973, USA*

¹⁰ *Peter Grünberg Institut and Institute for Advanced Simulation, Forschungszentrum Jülich and JARA, D-52425 Jülich, Germany*

Spin-polarized electrons confined in low-dimensional structures are of high interest for spintronics applications. Here, we investigate the electronic structure of an ordered array of Bi monomer and dimer chains on the Ag(110) surface. By means of spin-resolved photoemission spectroscopy, we find Rashba-Bychkov split bands crossing the Fermi level with one-dimensional constant energy contours. These bands are up-spin polarized for positive wave vectors and down-spin polarized for negative wave vectors, at variance with the Rashba-Bychkov model that predicts bands with opposite spin on each half of the surface Brillouin zone. Density functional theory shows that spin-selective hybridization with the Ag bulk bands originates this unconventional spin texture.

I. INTRODUCTION

The spin field-effect transistor proposed in the 1990s [1] opened a gateway to manipulate and use the spin of electrons for information technology [2, 3]. Although efficient manipulation of electron spins in semiconductors has been achieved [4, 5], reaching high spin-charge interconversion efficiency is still a challenge in spintronics research. An efficient conversion was reported in systems with strong spin-orbit interaction, either due to the Rashba-Bychkov (RB) effect in a two-dimensional (2D) electron gas [6, 7] or due to the spin-momentum locking in the surface states of topological insulators (TI) [8–12]. More recently, bulk systems with large spin-orbit splitting and one-dimensional (1D) electronic features were predicted to host exotic quantum phenomena [13–19]. In these systems, quasi-1D states exhibit a characteristic spin texture in k -space that is locked along the 1D Fermi surface between opposite directions, thus preventing electron backscattering and generating robust spin currents. The creation of 1D systems with large spin-orbit splitting has been partially explored in the growth of heavy elements on 110 surfaces, e.g. Bi/InAs(110) [20], Bi(Pb)/Cu(110)[21], Bi/Au(110)[22], Bi/GaSb(110)[23] and Pt/Si(110)[24]. These quasi-1D Rashba systems were experimentally reported to exhibit interesting electronic effects caused by the reduced dimensionality, in

particular nearly 1D contours, and giant conventional Rashba splitting. In conventional RB systems two channels of opposite spins are present at negative as well as at positive wave vectors [25, 26]. This leads to a partial spin compensation and a decrease of the spin-to-charge conversion efficiency [8]. Differently, in the surface states of a TI there is only one spin channel at negative (positive) wave vectors, hence providing a better spin-charge conversion efficiency. A similar scenario, where the Fermi contour consists of only one parallel line of opposite spin direction with respect to $\bar{\Gamma}$, has been experimentally reported for Bi high indexed surfaces [27–29], originating from the topological properties of Bi surface states.

Here, by spin-resolved photoemission experiments and first-principles calculations we show that, due to the RB effect, the Bi/Ag(110) $p(4\times 1)$ superstructure hosts a similar, unconventional, spin texture. The present system exhibits a 1D structural anisotropy and, at the Fermi level (E_F), a couple of states with nearly 1D contours, with only up (down) spin channel for positive (negative) wave vectors. This unconventional RB spin texture provides, on related insulating substrates, the analogous of a quantum spin-Hall effect [30], offering new perspectives for 1D spin-polarized electron transport.

II. METHODS

The Ag(110) crystal was prepared by sputtering and annealing cycles. Bi was evaporated from a BN basket at a rate of 0.25 ML/min. Bi on Ag(110) forms, similarly to Bi on Cu(110), different reconstructions. Slightly below 0.5 ML the surface shows a $c(2\times 2)$ reconstruction, which

*E-mail address: daniela.pacile@fis.unical.it

†Present address: Elettra - Sincrotrone Trieste, S.S. 14 km 163.5 in AREA Science Park, Basovizza, I-34149 Trieste, Italy

becomes $p(4\times 1)$ at about 0.75 ML. Annealing at about 400 K for 30 minutes results in sharper spots and a lower background in LEED. Figure 1b shows the LEED pattern, where yellow circles mark the 1×1 spots of Ag(110) separated by three spots due to the $\times 4$ reconstruction along the $[1\bar{1}0]$ direction.

Angle-Resolved Photoemission Spectroscopy (ARPES) measurements were performed at the VUV photoemission and at the NanoESCA[31] beamlines of the Elettra synchrotron, at $T=90\text{K}$, using a hemispherical analyser and a momentum microscope, respectively. The microscope at the NanoESCA beamline is equipped with a W(001)-based spin detector [32], which enables collecting constant energy spin-resolved maps in a $[k_x, k_y]$ range of $[-2,2]\text{\AA}^{-1}$. The analysis of the spin-resolved data was performed following the procedure described in [33]. The SQA was aligned with the beam incidence direction and the sample was rotated with respect to the beam, as shown in Supplemental Material, Fig. S1(a). Additional spin-polarized ARPES spectra were acquired at the U5UA beamline at the National Synchrotron Light Source (NSLS) [34]. Scanning Tunneling Microscopy (STM) was conducted at the Elettra APE beamline. The topographic images were acquired in a constant current mode at room temperature (RT). The calculations have been performed within density functional theory (DFT) in the generalized gradient approximation [35], employing the full potential linearized augmented plane-wave method as implemented in the Fleur code [www.flapw.de]. For the band structure calculations we use a 20 layer Ag(110) film with the upper half relaxed and terminated with Bi rows, as shown in Fig. 1d. The product of plane-wave cutoff and muffin-tin radius is 9.0 and 24 k-points have been used for the self-consistent calculations.

III. RESULTS AND DISCUSSION

The structural properties of the Bi/Ag(110) $p(4\times 1)$ superstructure have been investigated by Low Energy Electron Diffraction (LEED) and Scanning Tunneling Microscopy (STM). Fig. 1a-b show the LEED patterns of clean Ag(110) and Bi/Ag(110) surfaces. The STM images, Fig. 1c, corresponding to the LEED pattern in Fig. 1b, shows highly oriented *single atom* chains running along the $[001]$ direction of the substrate, regularly separated by upper *double atoms* chains, of approximately 2.9 Å lateral length (see line profile of panel d). From the line profiles reported in Fig. 1d-e, the apparent vertical displacement within upper and lower Bi chains is estimated to be of about 1.0 Å and the step edge between adjacent Ag(110) terraces of about 1.65 Å, consistently with the interplanar distance of Ag(110) (1.46 Å calculated here within the generalized gradient approximation).

Density functional theory (DFT), based on the STM topographic images, derives the relaxed geometry depicted in Fig. 1f, which agrees with the experimental

data. The surface unit cell (yellow rectangle) contains two types of inequivalent Bi atoms. At the corner sites of the cell, Bi atoms occupy a substitutional site in the topmost Ag layer. These alloyed atoms form parallel rows along the $[001]$ direction, as also deduced from STM data. Between two adjacent alloyed Bi rows (Bi¹ atoms), a couple of Bi overlayer rows (Bi² dimers) are identified, with relative distance from Bi¹ of $\Delta z=1.41$ Å, consistently with the atomic structure of Bi/Cu(110)[21].

In Fig. 2a we report ARPES data measured along $\bar{\Gamma}-\bar{Y}$ of the Surface Brillouin Zone (SBZ) of the $p(4\times 1)$ superstructure, i. e. along the chain direction $[001]$ (Fig. 2f) aligned with the light polarization vector (see Fig. S1a of the Supplemental Material). We identify two states marked with R₁ and R₂ and a third state, R₃, which is better visible in the second SBZ (Fig. 2b). We mark them by blue contours on the left side of $\bar{\Gamma}$, and by red colour their counterpart on the right side. Figure 2d-e show 2D momentum maps taken at 0.55 eV binding energy. In this experimental conditions the Ag bands have a dogbone-like shape (Fig. S1b of the Supplemental Material), whose only the part of arc-like shapes remains weakly visible. The main features arising from the Bi superstructure (Fig. 2e) are three states running along k_y near the center of the SBZ, corresponding to R₁, R₂ and R₃. While R₁ is nearly straight, R₂ and R₃ display a k-modulation, very weak for R₂ and stronger for R₃, with a period corresponding to the SBZ periodicity. We focus on the contours of R₁ and R₂ that closely approach an ideal 1D character.

Fig. 2g shows the spin character of the Bi-related states, measured with the Spin Quantization Axis (SQA) aligned along the $\bar{\Gamma}-\bar{X}$ direction (see Methods section for more details). The spin-resolved data show that the R₁ and R₂ states have an unconventional spin texture, i.e. the same spin at negative k_x , and opposite for positive k_x values. Specifically, for the R₁ state the in-plane polarization is fully along k_y , that is parallel to the Fermi contour, as confirmed by spin measurements taken with the SQA along the $\bar{\Gamma}-\bar{Y}$ direction (Fig. S2 of the Supplemental Material). The profiles and spin polarization of the R₁ and R₂ states are similar to the ones expected for the 1D edge states of a 2D topological material. Spin-resolved ARPES on the topological metallic states of Bi(114) [27, 28], display a very linear spin texture, with a single band instead of the pair in the present system. In the following, we show that although the states here observed appear very similar to the one in refs [27, 28] their origin is different.

By changing the sample's orientation with respect to the light polarization direction (see Methods section and Fig. S1a of the Supplemental Material) other Bi-induced states are observed, as shown in Fig. 3a. Prominent states, R₄ and R₅ pairs, appear at higher binding energies. We notice that these states have little dispersion along $\bar{\Gamma}-\bar{Y}$ (Fig. 3b), i.e. along the chain direction. Fig. 3c-d display the spin-integrated and spin-resolved 2D momentum maps acquired at 3.0 eV binding energy

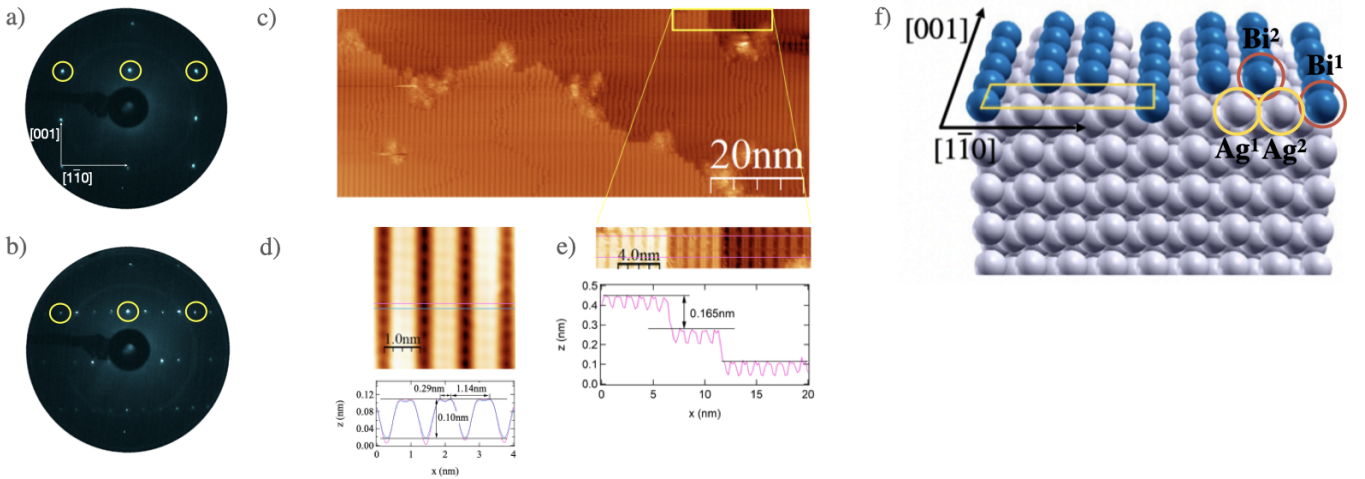


FIG. 1: LEED images taken with electron energy of 72 eV of: (a) clean Ag(110); (b) Bi/Ag(110) $p(4\times 1)$. (c-e) STM images on different length scales of the sample in (b) acquired with constant-current mode (bias voltage was -380mV and tunneling current 1 nA). Line profiles extracted from d) and e) images along the pink and light blue lines, marking the apparent width and vertical displacement of the chains, as well as the step edge between adjacent Ag(110) terraces, are shown. (f) Schematics of the surface structure. The yellow rectangle is the surface unit cell. Bi¹ and Bi² are Bi atoms in substitutional sites and in the topmost layer, respectively. Ag¹ and Ag² are Ag atoms of the topmost substrate layer, slightly rumbled due to the Bi atomic chains.

(note that the SQA is now aligned along $\bar{\Gamma}$ - \bar{Y} , as shown in Fig. 3e), showing the contours of R₅ state repeated according to four-fold periodicity. We notice an unconventional spin pattern with one spin channel on the left side of $\bar{\Gamma}$ and opposite on the right, as sketched in Fig. 3e. A similar texture is observed also for the R₄ state (Fig. S3 in the Supplemental Material).

In order to discuss these findings, we present DFT calculations for the electronic states of the Bi/Ag(110) $p(4\times 1)$ system along the chain direction $\bar{\Gamma}$ - \bar{Y} (Fig. 4a). We observe four pairs of nearly parabolic spin-orbit split bands crossing at $\bar{\Gamma}$ at 0.1, -0.2, -1.0 and -1.7 eV. We identify with R₁, R₂, R₃ the lowest three pairs of bands. These bands correspond to the experimentally observed R₁, R₂ and R₃ states beside a discrepancy in the energy position, both along $\bar{\Gamma}$ - \bar{Y} and \bar{X} - \bar{S} directions (Fig. S4(a) in the Supplemental Material shows theoretical results along \bar{X} - \bar{S} direction). In agreement with the experiment, R₁ and R₂ states are the most intense features with same position in k_x between $\bar{\Gamma}$ - \bar{Y} and \bar{X} - \bar{S} direction, leading to nearly linear contours in the constant energy cuts. On the other hand, the binding energy position of R₃ varies, leading to the observed undulations. Focusing on the second pair, R₂, from a parabolic fit around the vertex, we extract a shift of the band maximum away from $\bar{\Gamma}$ -point of about $k_0=0.035\text{\AA}^{-1}$, corresponding to a Rashba parameter of $\alpha=1.65\text{ eV\AA}$ and comparable to the giant spin splitting of the Bi_{*x*}Pb_{*1-x*}Ag₂ surface alloy [36]. Moreover, the k_0 value here extracted is close to the maximum momentum splitting measured at the border of the BZ in the Bi/Cu(110) $p(4\times 1)$ system, $2k_0=(0.075\pm 0.05)\text{\AA}^{-1}$ [21]. In Fig. 4a we also notice two weakly dispersive states with positive effective mass,

located at $\bar{\Gamma}$ -point at about 1.4 eV and 2.4 eV, respectively. They are clearly visible in the experimental results of Fig. 3b and correspond to R₄ and R₅ states, beside a discrepancy in the energy position.

In Fig. 4b we show the theoretical band structure in the perpendicular direction $[\bar{1}\bar{1}0]$, i.e. along $\bar{\Gamma}$ - \bar{X} . The R₂ pair crosses above E_F and form two parabola with positive effective mass. We can estimate a Rashba parameter of about $\alpha=0.55\text{ eV\AA}$, much smaller than the one extracted along the $\bar{\Gamma}$ - \bar{Y} direction, where there is higher electron mobility. We furthermore notice that the R₂ pair shows a saddle-like shape in k -space, similar to what has been observed in deeply lying RB split Ag(111) and Au(111) surface states located at \bar{M} [37]. In the binding energy range between 0 and 1 eV below E_F , the R₁-R₃ states form open contours, thus we only observe Ag states arising from the $\times 4$ folding. Above 1.0 eV binding energy, in line with the experimental results of Fig. 3, we find several spin-split bands belonging to Bi, among which we select the R₄ and R₅ pairs with crossing point at about 1.4 eV and 2.3 eV, respectively. As a result of the comparison with Fig. 4a, we point out that these deeper lying states are mainly dispersive along the perpendicular direction, where, indeed, they exhibit sizable RB splitting and electron mobility. Instead, in agreement with the experiment, these states are nearly non-dispersive along $\bar{\Gamma}$ - \bar{Y} (Fig. 4a), and cause the observed kinks when intersecting the higher Bi states, as seen in Fig. 2a and Fig. 3b.

DFT calculations explain the origin of the particular spin texture for R₁ and R₂, as well as for R₄ and R₅ states. In Fig. 4c we show surface projected Ag(110) bands folded according to the 4×1 periodicity. Here, a

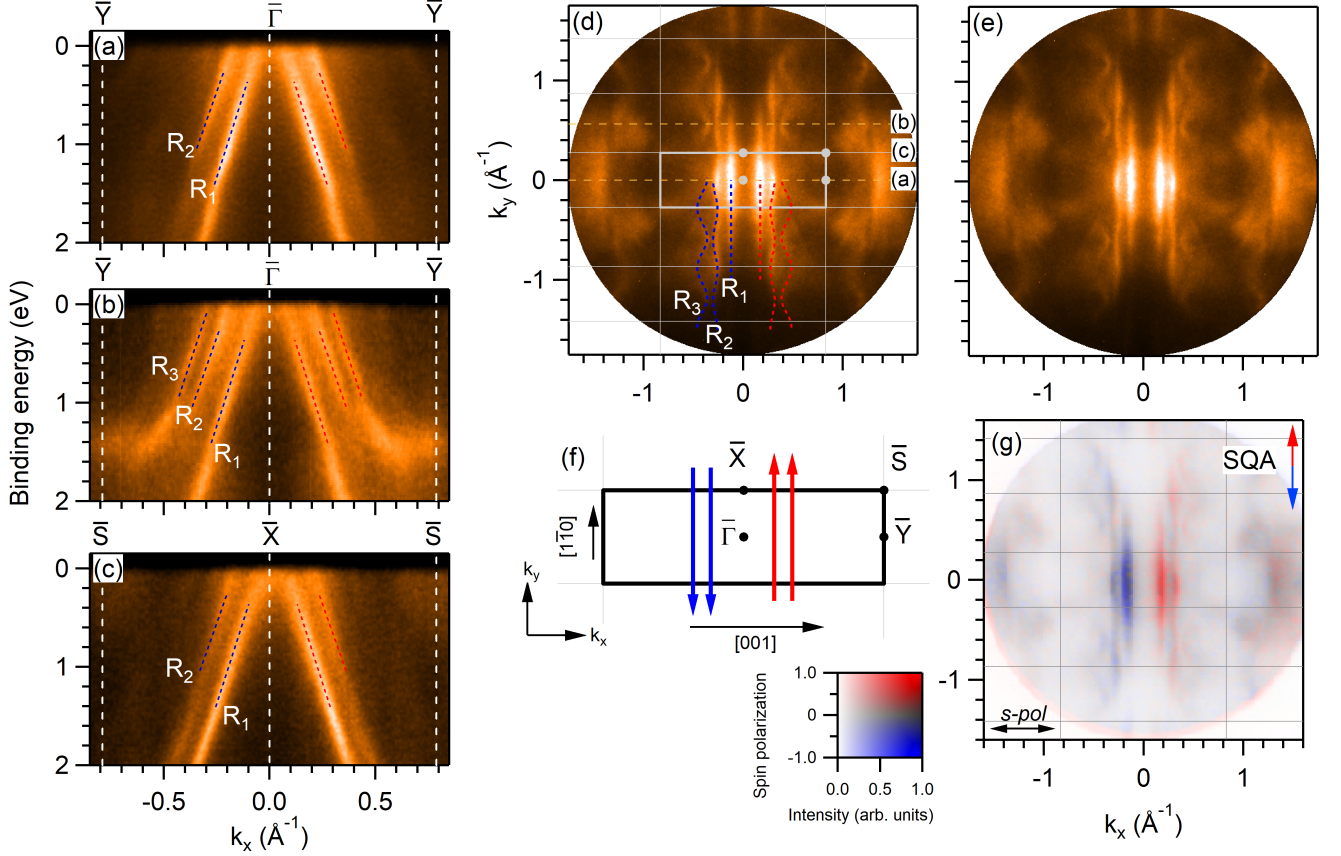


FIG. 2: Energy-momentum dispersion of Bi/Ag(110) $p(4\times 1)$ along: (a) $\bar{\Gamma}$ - \bar{Y} of the first SBZ; (b) $\bar{\Gamma}$ - \bar{Y} of the second SBZ; (c) along \bar{X} - \bar{S} ; the corresponding k_y positions of the cuts are indicated in panel d. (d-e) 2D momentum maps taken at 0.55 eV binding energy with and without SBZ on top. Blue and red dashed lines indicate R_1 - R_3 couple of RB states. Solid grey lines indicate the SBZ. (f) SBZ of Bi/Ag(110) $p(4\times 1)$. The sketch of blue and red arrows show the spin texture at the Fermi surface from this work. (g) Spin-resolved photoemission intensities for the data shown in panel (e). Red and blue intensities correspond to majority and minority electronic states as shown in the legend. All measurements were taken at 120 eV of photon energy with s -polarized light. The directions of the light polarization and of the SQA are shown in panel (g).

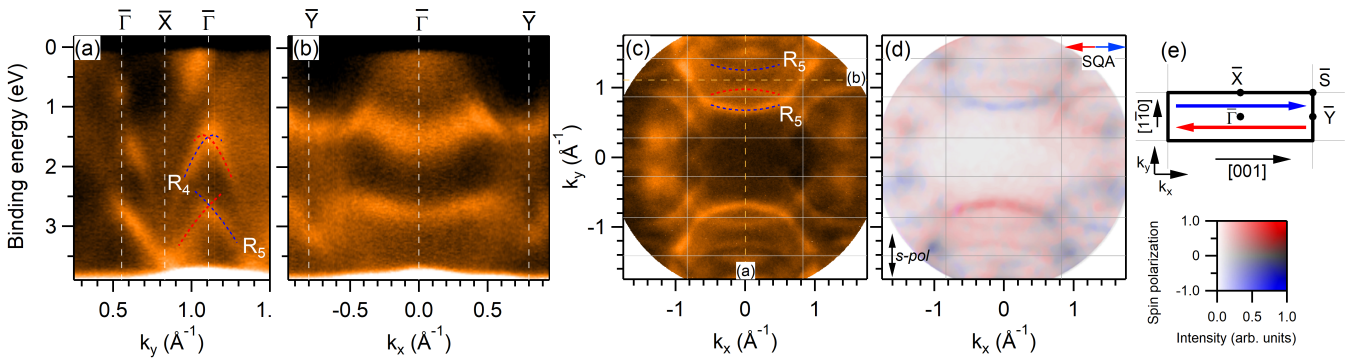


FIG. 3: (a,b) Energy-momentum dispersion of Bi/Ag(110) $p(4\times 1)$: (a) along $\bar{\Gamma}$ - \bar{X} direction; (b) along $\bar{\Gamma}$ - \bar{Y} direction. The corresponding k_y and k_x positions of the cuts are indicated in the panel (c). (c) 2D momentum map, taken at 3.0 eV binding energy. (d) Spin-resolved photoemission intensities of the data shown in panel (c). Blue and red dashed lines indicate R_4 - R_5 couple of RB states. Solid grey lines indicate the SBZ. All measurements were taken at 120 eV of photon energy with s -polarized light. (e) SBZ of Bi/Ag(110) $p(4\times 1)$. The sketch of blue and red arrows show the spin texture at about 3.0 eV binding energy from this work.

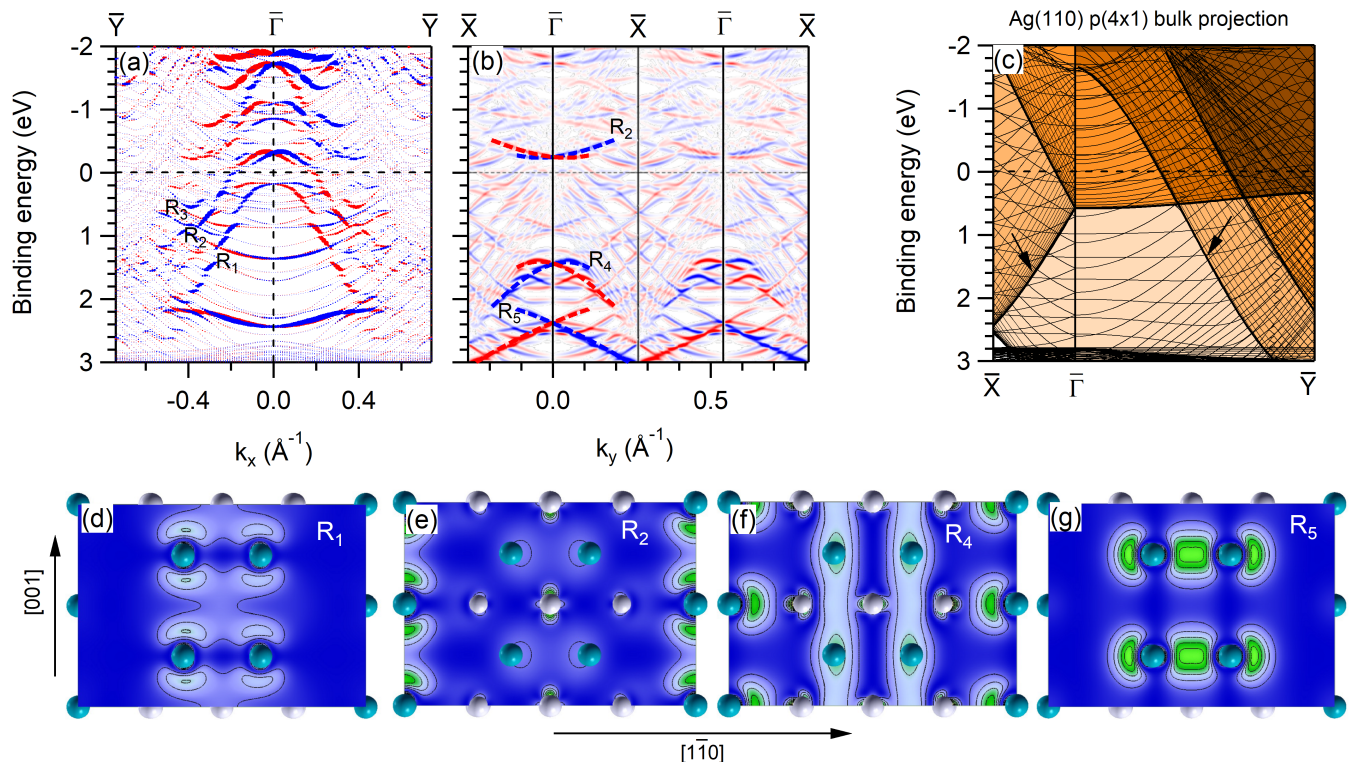


FIG. 4: (a) Theoretical band structure of Bi/Ag(110) $p(4\times 1)$ parallel to the Bi chains, that is along $\bar{\Gamma}-\bar{Y}$. The color and size of the symbols indicate the orientation and size of the spin-polarization at the Bi atoms in k_y direction. (b) The same representation perpendicular to the Bi chains, i. e. along $\bar{\Gamma}-\bar{X}$, with SQA referred to k_x direction. (c) Ag(110) bands along $\bar{\Gamma}-\bar{X}$ and $\bar{\Gamma}-\bar{Y}$ folded according to the 4×1 periodicity. Different colors indicate a different density of states. (d-g) Charge density plots of states R_1 (d), R_2 (e), R_4 (f) and R_5 (g) pairs in the plane of the Bi^2 dimers (d, g) or the Bi^1 alloyed atoms (e, f). (d, e) are extracted at 0.6 eV; (f) at 1.4 eV; (g) at 2.3 eV binding energy. Bi atoms are shown in blue, Ag atoms in grey.

step-like increase in the density of Ag states is expected going farther from $\bar{\Gamma}$ -point, both along $\bar{\Gamma}-\bar{X}$ and $\bar{\Gamma}-\bar{Y}$ directions. Several zones with different density of states can be identified, as highlighted by different color. A bright zone close to $\bar{\Gamma}$, delimited by two lines marked by black arrows, has relatively low density of Ag states. When Bi atoms are accounted for, the inner branch of a RB pair (e.g., R_1 at negative wave vectors) remains within this zone and has little hybridization with Ag states. The outer branch (such as R_1 at positive wave vectors) due to its lower group velocity enters the zone with dense Ag states, just below E_F , thus hybridizing with the Ag states. For this reason, both along $\bar{\Gamma}-\bar{X}$ and $\bar{\Gamma}-\bar{Y}$, for each couple of Bi states the inner spin-split band is visible in the simulations as well as in the experiments, while the outer one strongly hybridizes with the Ag bulk states, leading to one single band for positive (negative) k values.

Fig. 4(d-g) show charge density plots of the Bi-derived states, all having p -character. The R_1 and R_2 states are oriented along the chain direction $[001]$ (Fig. 4d-e), and exhibit 1D dispersion character. We point out that the R_1 state is localized on Bi dimer rows, while the R_2 state is centered on the alloyed Bi rows. We notice

that R_1 state, at variance with R_2 , shows a significant hybridization with the Ag states (see Fig. S4(b-c) of the Supplemental Material). The R_4 and R_5 are mainly oriented along the $[\bar{1}10]$ direction (Fig. 4f-g). The R_5 is fully localized at Bi^2 dimers along $[\bar{1}10]$ direction and with small overlap along the chains direction. The R_4 shows a more complex behavior, mostly located at Bi^1 alloyed atoms but with non negligible extension along both directions. The strong anisotropy of Bi states shown here explains why by changing the light polarization one can selectively excite one couple (R_1 and R_2 in Fig. 2) or the other (R_4 and R_5 in Fig. 3).

Finally, we comment on the perspectives of the present results for spintronics applications. The present superstructure provides a model system demonstrating theoretical and experimental realization of such spin texture. Our study may stimulate further exploration of similar systems grown on insulating substrates, being useful for energy-efficient spintronic applications.

IV. CONCLUSIONS

We report on quasi-1D atomic and electronic structure with unconventional RB spin texture observed in Bi/Ag(110) $p(4\times 1)$ superstructure. Using ARPES we show that the Fermi surface displays a pair of linear states strongly localized on the chains and dispersing along the chain direction. Spin-resolved photoemission spectroscopy on these states shows that only up (down) spin channel is present at positive (negative) wave vectors. We support our findings by DFT calculations, which explain the current spin texture as originating from the k -dependent hybridization of the Bi-derived RB bands with the Ag bulk states. The present non-conventional

spin texture, together with quasi-1D shape, may support the realization of spintronic devices based on spin-charge interconversion.

Acknowledgements

We acknowledge EUROFEL-ROADMAP ESFRI of the Italian Ministry of Education, University and Research. G.B. gratefully acknowledges the computing time granted through JARA-HPC on the supercomputer JU-RECA at Forschungszentrum Jülich. This work is supported by the German Federal Ministry of Education and Research (BMBF) under Grant No. 5K19PGA.

-
- [1] S. Datta and B. Das, *Applied Physics Letters* **56**, 665 (1990).
- [2] D. D. Awschalom and M. E. Flatté, *Nature Physics* **3**, 153 (2007).
- [3] P. Chuang, S.-C. Ho, L. W. Smith, F. Sfigakis, M. Pepper, C.-H. Chen, J.-C. Fan, J. P. Griffiths, I. Farrer, H. E. Beere, G. A. C. Jones, D. A. Ritchie, and T.-M. Chen, *Nature Nanotechnology* **10**, 35 (2015).
- [4] H. C. Koo, J. H. Kwon, J. Eom, J. Chang, S. H. Han, and M. Johnson, *Science* **325**, 1515 (2009).
- [5] I. Appelbaum, B. Huang, and D. J. Monsma, *Nature* **447**, 295 (2007).
- [6] J. C. R. Sánchez, L. Vila, G. Desfonds, S. Gambarelli, J. P. Attané, J. M. De Teresa, C. Magén, and A. Fert, *Nature Communications* **4**, 2944 (2013).
- [7] E. Lesne, Y. Fu, S. Oyarzun, J. C. Rojas-Sánchez, D. C. Vaz, H. Naganuma, G. Sicoli, J. P. Attané, M. Jamet, E. Jacquet, J. M. George, A. Barthélémy, H. Jaffrès, A. Fert, M. Bibes, and L. Vila, *Nature Materials* **15**, 1261 (2016).
- [8] R. Sun, S. Yang, X. Yang, E. Vetter, D. Sun, N. Li, L. Su, Y. Li, Y. Li, Z.-z. Gong, Z.-k. Xie, K.-y. Hou, Q. Gul, W. He, X.-q. Zhang, and Z.-h. Cheng, *Nano Letters* **19**, 4420 (2019).
- [9] Y. Shiomi, K. Nomura, Y. Kajiwara, K. Eto, M. Novak, K. Segawa, Y. Ando, and E. Saitoh, *Physical Review Letters* **113**, 196601 (2014).
- [10] J.-C. Rojas-Sánchez, S. Oyarzún, Y. Fu, A. Marty, C. Vergnaud, S. Gambarelli, L. Vila, M. Jamet, Y. Ohtsubo, A. Taleb-Ibrahimi, P. Le Fèvre, F. Bertran, N. Reyren, J.-M. George, and A. Fert, *Phys. Rev. Lett.* **116**, 096602 (2016).
- [11] J. Han, A. Richardella, S. A. Siddiqui, J. Finley, N. Samarth, and L. Liu, *Phys. Rev. Lett.* **119**, 077702 (2017).
- [12] K. Kondou, R. Yoshimi, A. Tsukazaki, Y. Fukuma, J. Matsuno, K. S. Takahashi, M. Kawasaki, Y. Tokura, and Y. Otani, *Nature Physics* **12**, 1027 (2016).
- [13] R. Noguchi, T. Takahashi, K. Kuroda, M. Ochi, T. Shirasawa, M. Sakano, C. Bareille, M. Nakayama, M. D. Watson, K. Yaji, A. Harasawa, H. Iwasawa, P. Dudin, T. K. Kim, M. Hoesch, V. Kandyba, A. Giampietri, A. Barinov, S. Shin, R. Arita, T. Sasagawa, and T. Kondo, *Nature* **566**, 518 (2019).
- [14] R. Noguchi, M. Kobayashi, Z. Jiang, K. Kuroda, T. Takahashi, Z. Xu, D. Lee, M. Hirayama, M. Ochi, T. Shirasawa, P. Zhang, C. Lin, C. Bareille, S. Sakuragi, H. Tanaka, S. Kunisada, K. Kurokawa, K. Yaji, A. Harasawa, V. Kandyba, A. Giampietri, A. Barinov, T. K. Kim, C. Cacho, M. Hashimoto, D. Lu, S. Shin, R. Arita, K. Lai, T. Sasagawa, and T. Kondo, *Nature Materials* **20**, 473 (2021).
- [15] L. Qiao, X. Xiong, H. Yang, D. Chen, Y. Li, J. Li, X. Peng, Z. Xu, J. Han, W. Xiao, and Y. Yao, *The Journal of Physical Chemistry C* **125**, 22312 (2021).
- [16] J. I. Pascual, G. Bihlmayer, Y. M. Koroteev, H.-P. Rust, G. Ceballos, M. Hansmann, K. Horn, E. V. Chulkov, S. Blügel, P. M. Echenique, and P. Hofmann, *Phys. Rev. Lett.* **93**, 196802 (2004).
- [17] P. Segovia, D. Purdie, M. Hengsberger, and Y. Baer, *Nature* **402**, 504 (1999).
- [18] D. Sánchez-Portal, S. Riikonen, and R. M. Martin, *Phys. Rev. Lett.* **93**, 146803 (2004).
- [19] I. Barke, F. Zheng, T. K. Rügheimer, and F. J. Himpsel, *Phys. Rev. Lett.* **97**, 226405 (2006).
- [20] T. Nakamura, Y. Ohtsubo, Y. Yamashita, S.-i. Ideta, K. Tanaka, K. Yaji, A. Harasawa, S. Shin, F. Komori, R. Yukawa, K. Horiba, H. Kumigashira, and S.-i. Kimura, *Phys. Rev. B* **98**, 075431 (2018).
- [21] A. Crepaldi, G. Bihlmayer, K. Kern, and M. Grioni, *New Journal of Physics* **15**, 105013 (2013).
- [22] A. Crepaldi, C. Tournier-Colletta, M. Pivetta, G. Autès, F. Patthey, H. Brune, O. V. Yazyev, and M. Grioni, *Phys. Rev. B* **88**, 195433 (2013).
- [23] Y. Ohtsubo, N. Tokumasu, H. Watanabe, T. Nakamura, P. Le Fèvre, F. m. c. Bertran, M. Imamura, I. Yamamoto, J. Azuma, K. Takahashi, and S.-i. Kimura, *Phys. Rev. B* **101**, 235306 (2020).
- [24] J. Park, S. W. Jung, M.-C. Jung, H. Yamane, N. Kosugi, and H. W. Yeom, *Phys. Rev. Lett.* **110**, 036801 (2013).
- [25] M. Kopciuszynski, M. Krawiec, R. Zdyb, and M. Jaochowski, *Scientific Reports* **7**, 46215 (2017).
- [26] A. N. Mihalyuk, L. V. Bondarenko, A. Y. Tupchaya, T. V. Utas, Y. E. Vekovshinin, D. V. Gruznev, S. V. Ereemeev, A. V. Zotov, and A. A. Saranin, *Phys. Rev. B* **104**, 125413 (2021).
- [27] P. Hofmann, M. M. Ugeda, A. Tamtögl, A. Ruckhofer, W. E. Ernst, G. Benedek, A. J. Martínez-Galera,

- A. Stróżecka, J. M. Gómez-Rodríguez, E. Rienks, M. F. Jensen, J. I. Pascual, and J. W. Wells, *Phys. Rev. B* **99**, 035438 (2019).
- [28] J. W. Wells, J. H. Dil, F. Meier, J. Lobo-Checa, V. N. Petrov, J. Osterwalder, M. M. Ugeda, I. Fernandez-Torrente, J. I. Pascual, E. D. L. Rienks, M. F. Jensen, and P. Hofmann, *Phys. Rev. Lett.* **102**, 096802 (2009).
- [29] M. Bianchi, F. Song, S. Cooil, A. F. Monsen, E. Wahlström, J. A. Miwa, E. D. L. Rienks, D. A. Evans, A. Strozecka, J. I. Pascual, M. Leandersson, T. Balasubramanian, P. Hofmann, and J. W. Wells, *Phys. Rev. B* **91**, 165307 (2015).
- [30] C. Brüne, A. Roth, H. Buhmann, E. M. Hankiewicz, L. W. Molenkamp, J. Maciejko, X.-L. Qi, and S.-C. Zhang, *Nature Physics* **8**, 485 (2012).
- [31] C. Schneider, C. Wiemann, M. Patt, V. Feyer, L. Plucinski, I. Krug, M. Escher, N. Weber, M. Merkel, O. Renault, and N. Barrett, *Journal of Electron Spectroscopy and Related Phenomena* **185**, 330 (2012).
- [32] C. Tusche, M. Ellguth, A. A. Ünal, C.-T. Chiang, A. Winkelmann, A. Krasnyuk, M. Hahn, G. Schönhense, and J. Kirschner, *Applied Physics Letters* **99**, 032505 (2011).
- [33] C. Tusche, M. Ellguth, A. Krasnyuk, A. Winkelmann, D. Kutnyakhov, P. Lushchik, K. Medjanik, G. Schönhense, and J. Kirschner, *Ultramicroscopy* **130**, 70 (2013), Eighth International Workshop on LEEM/PEEM.
- [34] E. Vescovo, H.-J. Kim, Q.-Y. Dong, G. Nintzel, D. Carlson, S. Hulbert, and N. V. Smith, *Synchrotron Radiation News* **12**, 10 (1999).
- [35] J. P. Perdew, K. Burke, and M. Ernzerhof, *Phys. Rev. Lett.* **77**, 3865 (1996).
- [36] C. R. Ast, D. Pacilé, L. Moreschini, M. C. Falub, M. Paganò, K. Kern, M. Grioni, J. Henk, A. Ernst, S. Ostanin, and P. Bruno, *Phys. Rev. B* **77**, 081407 (2008).
- [37] R. Requist, P. M. Sheverdyaeva, P. Moras, S. K. Mahatha, C. Carbone, and E. Tosatti, *Phys. Rev. B* **91**, 045432 (2015).